



# Calibration and uncertainty estimation of non-contact coordinate measurement systems based on Kriging models

Lan Fei<sup>a</sup>, Jean-Yves Dantan<sup>b,\*</sup>, Cyrille Baudouin<sup>b</sup>, Shichang Du<sup>a</sup>

<sup>a</sup> Department of Industrial Engineering and Management, School of Mechanical Engineering, Shanghai Jiaotong University, Shanghai, China

<sup>b</sup> LCFC, Arts et Métiers ParisTech, HESAM, Université de Lorraine, 4 rue Augustin Fresnel, 57078 Metz Cedex 3, France

## ARTICLE INFO

### Keywords:

Coordinate measurement system  
Non-contact measurement  
Measurement uncertainty  
Calibration  
Kriging model

## ABSTRACT

Non-contact three dimensional (3D) coordinate measurement systems (CMSs) using optical scanning techniques have the advantage of fast acquiring large numbers of points. However, these systems are known to be less accurate in comparison to the contact-based counterparts. To improve the measurement accuracy of non-contact 3D CMSs, a novel Kriging models-based calibration and uncertainty estimation method is proposed. The spatial correlation of measurement uncertainty is investigated and the calibration values for unmeasured points based on Kriging models are estimated. A procedure of best model selection is presented, and the influence of the calibration model parameters is analyzed. The proposed calibration method is validated through an ATOS II triple scan system. The results show that a significant accurate improvement for the non-contact 3D measurement system is achieved.

## 1. Introduction

Since three dimensional (3D) coordinate measurement systems (CMSs) with optical imaging devices offer the option to output high density data for parts at high speed, they have been widely used in lab and industry [1–4]. In recent years, non-contact optical measurement systems have not only been seen with significant advances in technical developments, but also undergone a boost in applications, such as surface quality improvement [5–8], surface error evaluation [9], surface separation [10,11], and tool wear monitoring [12]. However, for actual camera lenses, such as a fixed length lens, a zoom lens or even an expensive high-quality telecentric lens, image distortions unavoidably exist due to lens aberrations, misalignment of optical elements and non-parallelism between image plane and sensor plane [13–15]. Due to the non-uniform characteristics of camera lens distortion, actually the coordinates on object surface may cause different values in the sensor plane. Therefore, measurement results are usually affected by measurement uncertainty, which could lead to technical and economic risks in industrial applications.

Over the last 30 years, two different methods have been adopted to achieve high accuracy, namely, uncertainty avoidance and calibration. Uncertainty avoidance is the traditional method focusing on the reduction of possible uncertainty sources in the design and manufacturing processes [16]. Careful design and precise construction can reduce the uncertainty, but every subsequent micrometer/nanometer of uncertainty reduction will

cause an exponentially increasing cost. So it is practical to calibrate CMSs between the measurement coordinate and the actual object.

The calibration and uncertainty estimation method has been explored as a cost-effective method of improving the accuracy of CMSs [17–20]. Early developments in calibration are well described by Evans [21]. Some effective methods are reported in the literature to model and calibrate CMSs. These methods include polynomial models and autoregressive moving average models [22], homogeneous coordinate transformation (HTM) methods [23], neural network based methods [24–28], D-H models [29,30], fuzzy error interpolation techniques [31], iterative learning and decoupling methods [32,33], recursive least squares identification techniques [34], Monte Carlo method [35] and other analytical methods [36–41].

So far, limited research on the spatial statistics-based methods to model and calibrate CMSs considering the spatial correlation of the measurement data has been conducted. The spatial correlation arises frequently in data measured within certain intervals of space, and the data indeed exhibits a significant amount of positive autocorrelation [42]. Measurements are often spatially correlated because they are obtained in similar manufacturing conditions and related to similar properties of the machined material [43]. Spatial correlation is different from temporal correlation, which is usually represented via time series models. In fact, spatial correlation models allow one to represent contiguity in space rather than in time. Spatial statistics, e.g. Kriging method, is one of most important meta-models for describe spatial

\* Corresponding author.

E-mail address: [jean-yves.dantan@ensam.eu](mailto:jean-yves.dantan@ensam.eu) (J.-Y. Dantan).

<https://doi.org/10.1016/j.precisioneng.2019.02.004>

Received 3 September 2017; Received in revised form 21 December 2018; Accepted 6 February 2019

Available online 18 February 2019

0141-6359/ © 2019 Elsevier Inc. All rights reserved.

correlations in random field [44]. Detailed descriptions of existing research on Kriging meta-models are provided in a review [45].

The literature on spatial statistics-based calibration methods is sparse. A method based on Co-Kriging models to estimate the errors of the surface form not only concerning spatial correlation but also concerning the influence of machining conditions is developed in Ref. [46]. A spatial statistical method to design adaptive inspection plans for the geometric control of mechanical parts with CMSs is presented in Ref. [47]. The prediction uncertainty of geometric deviations is provided using Kriging models. A Kriging-based procedure to identify the minimum of measured points to check the conformity with a given confidence level in the inspection of large surfaces is presented in Ref. [48]. An on-line inspection system with error calibration to obtain high machining accuracy for free-form surface components is proposed in Ref. [49]. Through the spatial statistical analysis of the residual errors of a regression model, the errors are decomposed into systematic errors and random errors. The spatial error compensation methods for computer numerical control (CNC) machining center is proposed in Refs. [50,51].

In these last applications, Kriging-based procedure to improve inspection has proved to be effective. This paper develops a Kriging-based method to achieve the calibration and uncertainty estimation of non-contact 3D CMSs. The advantages of this proposed solution are many in comparison to the classical approaches:

- It is not necessary to develop a complex phenomenological model of the sensor. The systematic error of a simplified model of the sensor was corrected by the Kriging model.
- It is possible to adopt an adaptive approach for the calibration. Based on the uncertainty estimation of the kriging model, it is possible to identify the spatial area that should be recalibrated.

The proposed Kriging-based method for the calibration of non-contact 3D CMSs is presented in Section 2. An application of the approach is illustrated through a case study in Section 3.

## 2. The proposed calibration method

The aim of this proposed calibration method is to correct the systematic error of the simplified model of the sensor by a kriging model. To do so, a gauge is measured. It is important to know the geometrical characteristics of this gauge. In this application, the GOM gauges are used.

### 2.1. The calibration procedure

Fig. 1 shows the calibration procedure of a measurement system, and the main steps are described as follows.

Step 1. Obtaining measured points and theoretical reference points of the gauge. A measured point  $S$  obtained by 3D CMS is denoted as,

$$s_{i\text{-measured}} = (x_{i\text{-measured}}, y_{i\text{-measured}}, z_{i\text{-measured}}) \quad (1)$$

where  $x_{i\text{-measured}}, y_{i\text{-measured}}, z_{i\text{-measured}}$  are three dimensional coordinates of a measured point respectively. These values are obtained from the simplified model of the sensor.

Based on the geometrical characteristics of the gauge, the coordinate values of theoretical reference points are determined by an orthogonal projection of the measured points on the gauge surface. Each measured point is mapped into the corresponding theoretical reference point,

$$s_{i\text{-theoretic}} = (x_{i\text{-theoretic}}, y_{i\text{-theoretic}}, z_{i\text{-theoretic}}) \quad (2)$$

where  $x_{i\text{-theoretic}}, y_{i\text{-theoretic}}, z_{i\text{-theoretic}}$  are three dimensional coordinates of the theoretical reference points respectively.

Illustration: Case of the sphere (Fig. 1) - To define the theoretical reference points, the gauge sphere is fitted to the measured points and each measured point is projected on the fitted gauge sphere.

Step 2. Calculating the measurement errors. A measurement error is the distance between the measured point and theoretical reference point at each direction of the axis X, Y, and Z,

$$\Delta s_i = (\Delta x_i, \Delta y_i, \Delta z_i) = (x_{i\text{-measured}}, y_{i\text{-measured}}, z_{i\text{-measured}}) - (x_{i\text{-theoretic}}, y_{i\text{-theoretic}}, z_{i\text{-theoretic}}) \quad (3)$$

A measurement error is discrete in each measured point on the surface, which needs to be calibrated. It is necessary to use spatial interpolation method to estimate the whole surface of the new measured part surface to realize the calibration of 3D measurement systems. The measurement error estimation model is established and applied at any point of the whole standardized part surface.

Step 3. A Kriging model is used to estimate the calibration  $\Delta C_0 = (\Delta x_0, \Delta y_0, \Delta z_0)$  on the specified untried site  $s_0$  by the response. The measurement errors  $\Delta C_i = (\Delta x_i, \Delta y_i, \Delta z_i)$  at a set of measured points  $s_{i\text{-measured}} = (x_{i\text{-measured}}, y_{i\text{-measured}}, z_{i\text{-measured}})$  (see Fig. 2) are represented as,

$$\begin{aligned} \Delta x_0 &= u(x_{i\text{-measured}}, y_{i\text{-measured}}, z_{i\text{-measured}}) = u(s_{i\text{-measured}}) \\ \Delta y_0 &= v(x_{i\text{-measured}}, y_{i\text{-measured}}, z_{i\text{-measured}}) = v(s_{i\text{-measured}}) \\ \Delta z_0 &= w(x_{i\text{-measured}}, y_{i\text{-measured}}, z_{i\text{-measured}}) = w(s_{i\text{-measured}}) \end{aligned} \quad (4)$$

where  $u, v, w$  are the Kriging models with different regression models and correlation models respectively.

Step 4. The calibration of any areas can be estimated by the Kriging spatial interpolation model. Therefore, this estimation could be used to calibrate the measurement error for a new measurement, which realizes the goal of calibration of 3D CMSs.

### 2.2. Kriging-based calibration model

Kriging is one of most important spatial statistics-based stochastic process prediction methods used to produce contour maps of surfaces derived from regularly or irregularly scattered points in a space. Let  $D$  be the region of a standardized part surface where the calibration value of measurement error  $\Delta C$  is predicted. And  $n$  points  $\mathbf{s} = (s_1, s_2, \dots, s_n)$  are measured with  $s_i \in D$  for  $i = 1, 2, \dots, n$ . The measurement error  $\Delta C$  (see Fig. 3) can be represented as,

$$\Delta C(\mathbf{s}) = \mu(\mathbf{s}) + \delta(\mathbf{s}), \mathbf{s} \in D \quad (5)$$

where  $\mathbf{s}$  is the variable  $\mathbf{s} = [s_1, s_2, \dots, s_n]^T$ ,  $\Delta C(\cdot)$  is regionalized measurement error,  $\mu(\cdot)$  is the expectation of deterministic structure and  $\delta(\cdot)$  is a stationary random function with zero mean and known dependence structure.

In order to develop the calibration model, the form of the deterministic structure  $\mu(\cdot)$  can be specified by three types of Kriging models:

- The simple Kriging:  $\mu(\mathbf{s}) = \text{constant}$ . The constant is known.
- The ordinary Kriging:  $\mu(\mathbf{s}) = \beta_0$ . The constant is unknown and estimated from the data.
- The universal Kriging:  $\mu(\mathbf{s}) = \sum_{j=1}^p f_j(\mathbf{s})\beta_j$ . It is a polynomial function of order 1 (linear universal Kriging, LUK) and of order 2 (quadratic universal Kriging, QUK) at the location  $\mathbf{s}$  with three dimension  $x, y$  and  $z$ . And ordinary Kriging can be considered as a special universal Kriging with  $p = 1$  and  $f_1(\mathbf{s}) = 1$ .

The measurement error  $\Delta C(\mathbf{s})$  for  $\mathbf{s} \in D$  is considered as a



realization of a Gaussian random process:

$$\Delta C(\mathbf{s}) = \beta'f(\mathbf{s}) + \delta(\mathbf{s}) \quad (6)$$

where  $f(\mathbf{s}) = (f_1(\mathbf{s}), f_2(\mathbf{s}), \dots, f_p(\mathbf{s}))'$  is a set of specified trend functions and  $\beta = (\beta_1, \beta_2, \dots, \beta_p)'$  is a set of coefficients.

The measurement error  $\Delta C(\mathbf{s})$  satisfies a Gaussian random process with zero mean and stationary covariance.

$$\begin{aligned} E(\Delta C(\mathbf{s})) &= \beta'f(\mathbf{s}) \\ \text{Cov}(\Delta C(\mathbf{s}), \Delta C(\mathbf{s} + d)) &= \sigma_\delta^2 R(d, \theta) \end{aligned} \quad (7)$$

where  $\sigma_\delta^2$  is the process variance, and  $R$  is the stationary correlation function (SCF).

The SCF depends only on the displacement vector  $d$  between any pair of points in  $D$  and on a set of hyper-parameters  $\theta$ .

$$R(\theta, \mathbf{s}_i, \mathbf{s}_j) = \prod_{i,j=1}^n R_j(\theta, \mathbf{s}_i - \mathbf{s}_j) \quad (8)$$

Base on equations (2) and (3), the joint random variable, measurement error,  $(\Delta C(\mathbf{s}_0), \Delta C(\mathbf{s}_1), \Delta C(\mathbf{s}_2), \dots, \Delta C(\mathbf{s}_n))$  satisfies a multivariate normal function,  $N((f_0', F)\beta, \sigma_\delta^2 \Sigma)$  with

$$\Sigma = \begin{pmatrix} 1 & r_0' \\ r_0 & R \end{pmatrix} \quad (9)$$

where  $r_0$  is the correlation vector  $r(\mathbf{s}_0) = [R(\theta, \mathbf{s}_1, \mathbf{s}_0) \dots R(\theta, \mathbf{s}_m, \mathbf{s}_0)]^T$ , and  $R$  is the  $n \times n$  correlation matrix whose  $(i, j)$  element is  $R(\mathbf{s}_i - \mathbf{s}_j)$ .

According to the best unbiased estimate condition of Kriging method, the mean of estimation of the calibration value  $\Delta C(\mathbf{s})$  at the point  $\mathbf{s}_0$  is:

$$\mu_{\Delta \hat{C}}(\mathbf{s}_0) = \Delta \hat{C}(\mathbf{s}_0) = f(\mathbf{s}_0) \cdot \beta^* + r(\mathbf{s}_0) \cdot \gamma^* = f_0' \beta^* + r_0' R^{-1} (\Delta C^n - F \beta^*) \quad (10)$$

where  $f_0$  is the  $p \times 1$  vector of the trend functions in  $\mathbf{s}_0$ ,  $F$  is the  $n \times p$  matrix of  $\{f_j(\mathbf{s}_i)\}_{i=1, \dots, n, j=1, \dots, p}$  of the trend functions calculated in  $(\mathbf{s}_1, \mathbf{s}_2, \dots, \mathbf{s}_n)$ ,  $\beta$  is unknown coefficient, and it is generalized by LS estimator  $\hat{\beta}^* = (F' R^{-1} F)^{-1} F' R^{-1} \Delta C$ .

Moreover, a confidence index about the prediction, called the Kriging variance, is the mean squared error between the prediction  $\Delta \hat{C}(\mathbf{s})$  and the actual value  $\Delta C(\mathbf{s})$ . It is given by:

$$\sigma_{\Delta \hat{C}}^2(\mathbf{s}_0) = E((\Delta \hat{C}_0 - C(\mathbf{s}_0))^2) = \sigma_\delta^2 (1 - r_0' R^{-1} r_0 + g_0' (F' R^{-1} F)^{-1} g_0) \quad (11)$$

where  $g_0 = f_0 - F' R^{-1} r_0$ ,  $f_0: f(\mathbf{s}_0)$ ,  $r_0: r(\mathbf{s}_0)$ ;  $F: [f(\mathbf{s}_1) \dots f(\mathbf{s}_n)]$ ,  $R: [r(\mathbf{s}_1, \mathbf{s}_1) \dots r(\mathbf{s}_n, \mathbf{s}_n)]$  and  $\sigma_\delta^2$  is the variance of the process.

$$\sigma_\delta^2 = \frac{1}{m} (\Delta C - F \beta^*)' (\Delta C - F \beta^*) \quad (12)$$

Kriging is an exact interpolation method, so predictions made at any point  $\mathbf{s}$  give  $\Delta \hat{C}(\mathbf{s}) = \Delta C(\mathbf{s})$ . Thus, the Kriging variance is null at these points.

### 2.3. Cross-validation of calibration model

Cross-validation is a model validation technique for assessing how the results of a statistical analysis generalize to an independent data set. It is mainly used to estimate how accurately a predictive model performs in practice. In order to better realize the calibration of a measurement system, the cross-validation technique is applied to select the best regression model and correlation model.

Fig. 4 shows the procedure of cross-validation. Several points of the measurement errors (testing data) are temporarily eliminated and then the calibration values of the measurement systems are estimated by Kriging methods using the remaining data (training data). This operation is repeated for some or all points. Thus at any observation point, it is calculated by Kriging with an estimated value  $\Delta C^*$  and an estimation variance of Kriging  $\sigma_\delta^2$ .

The main steps are described as follows.

Step 1: Generate measurement error with three dimensions  $\Delta C_i = (\Delta x_i, \Delta y_i, \Delta z_i)$  by the  $N$  measured points and nominal points which are projected on the fitting surface obtained by LS method.

Step 2: Select  $M$  points as measured points for the estimation of calibration and temporarily eliminate the measurement error of the remaining  $(N-M)$  points.

Step 3: Calculate the estimation of calibration and Kriging variance associated in the remaining  $(N-M)$  points.

Step 4: Repeat  $q$  times by steps (2) to (3) for each of  $M$ .

Step 5: Calculate the cross-validation criterion.

Step 6: Build the box plot (box-whisker plot) for evaluation value of cross-validation criterion on the  $M$  points.

Once the cross-validation is performed, several important criterions are used to evaluate the performances of the different Kriging methods. Here is a list of the most popular cross-validation criterions.

$$\text{mean error: } ME = \frac{1}{n} \sum_{i=1}^n [\Delta C(s_i) - \Delta C^*(s_i)] \quad (13)$$

$$\text{mean squared error: } MSE = \frac{1}{n} \sum_{i=1}^n [\Delta C(s_i) - \Delta C^*(s_i)]^2 \quad (14)$$

$$\text{root mean squared error: } RMSE = \sqrt{\frac{1}{n} \sum_{i=1}^n [\Delta C(s_i) - \Delta C^*(s_i)]^2} \quad (15)$$

$$\text{average Kriging standard error: } AKSE = \sqrt{\frac{1}{n} \sum_{i=1}^n \sigma_\delta^2(s_i)} \quad (16)$$

$$\text{mean standardized prediction error: } MSPE = \frac{1}{n} \sum_{i=1}^n \frac{\Delta C(s_i) - \Delta C^*(s_i)}{\sigma_\delta(s_i)} \quad (17)$$

root mean square standardized prediction error

$$:RMSPE = \sqrt{\frac{1}{n} \sum_{i=1}^n \left[ \frac{\Delta C(s_i) - \Delta C^*(s_i)}{\sigma_\delta(s_i)} \right]^2} \quad (18)$$

where  $\Delta C(s_i)$  is the real measurement error in the site,  $\Delta C^*(s_i)$  is estimated calibration in the site,  $\sigma_\delta(s_i)$  is the Kriging standard variance value and  $n$  is the number of measured points used for the Kriging estimation.

The model is chosen if the cross-validation criterions satisfy:

- 1) Mean estimation errors (ME) and mean standardized prediction error (MSPE) are close to 0. This criterion ensures the absence of bias.
- 2) The variance of the estimation errors (MSE, RMSE) is lower. This criterion reflects the robustness of the estimation and it provides the information on the estimation accuracy.
- 3) The variance of the standard errors (RMSPE) is closer to 1. It indicates that the standard deviation of Kriging properly reflects the estimation accuracy.

### 3. Applications

In this section, several experiments were conducted to illustrate how the proposed method based on Kriging calibrates a 3D measurement system and realize the measurement more precise. The calibration evaluation is analyzed with the comparison for ordinary Kriging and universal Kriging.

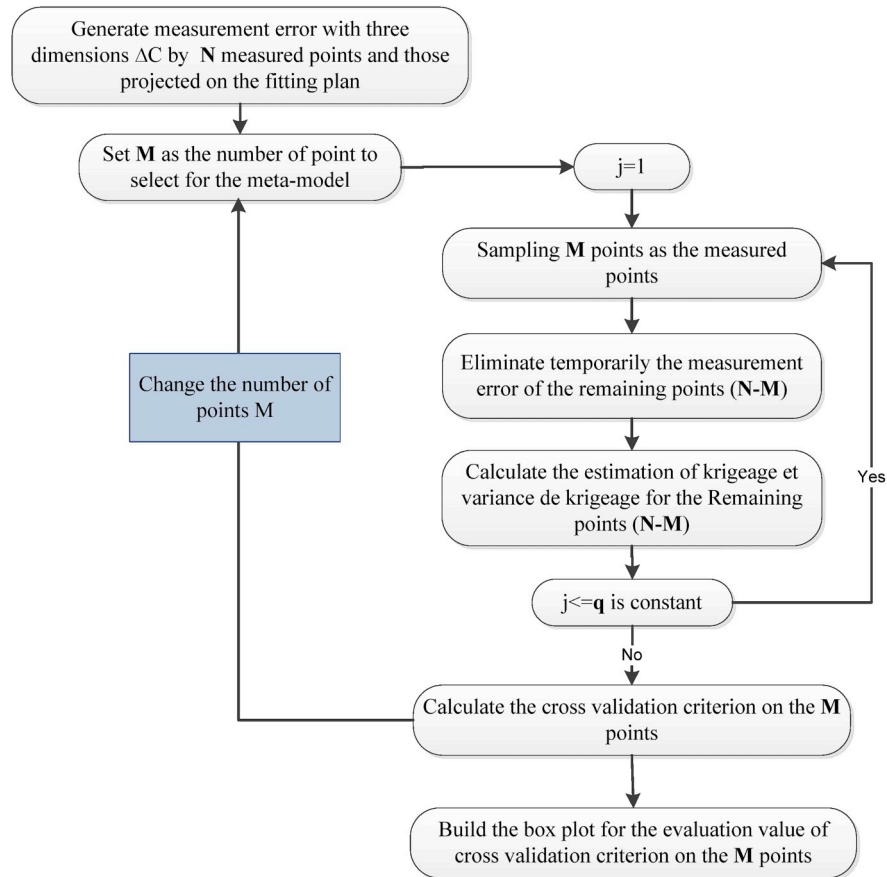


Fig. 4. Procedure of cross validation.

### 3.1. Experimental setup

The stereoscopic sensor (ATOS II Triple Scan, GOM) is installed on the manipulator (Fig. 5), which can be used to scan complex surfaces. The measurement system GOM is calibrated through the proposed calibration method based on a simplified phenomenological model of the



Fig. 5. Measurement system ATOS II TS GOM.

sensor.

The experiment measurements were executed on the planes of gauge (see Fig. 6) and spheres of the gauge (see Fig. 7). To eliminate the influence of plane position, different positions of planes were measured by the sensor GOM: lower plane, middle plane, upper plane (blue), and diagonal plane (green) shown in Fig. 6.

### 3.2. Calculate measurement uncertainty

In order to reduce systematic errors and realize calibration of the GOM measurement system, it is firstly important to calculate measurement error on the surfaces.

#### 3.2.1. Plane case

To model the calibration of the GOM sensor on the datum plane,  $\Delta z$ , or  $\Delta z$  and  $\Delta y$  are represented as the measurement error corresponding to the different positions of the plane. For lower, middle, and upper planes inclined with small angle (less than  $10^\circ$ ),  $\Delta z$  is used to represent the calibrations, and for the diagonal plane inclined with large angle (around  $45^\circ$ ),  $\Delta z$  and  $\Delta y$  are all used to represent the calibrations (see Fig. 8).

In Fig. 8, large dots are known as the measure, and the gauge plane is represented by the line. For the inclined plane with small angle,  $\Delta z$  are the differences between the measured points and projection points on the gauge plane. For inclined plane with large angle,  $\Delta z$  and  $\Delta y$  are the differences between the measured points (black) and projection points on the gauge plane.

The measured points in three dimensions  $S_{i-\text{measured}} = (x_{i-\text{measured}}, y_{i-\text{measured}}, z_{i-\text{measured}})$  were obtained by GOM sensor on the four planes. The gauge planes are shown in Table 1.

According to equation (9) and Fig. 8, the measurement errors

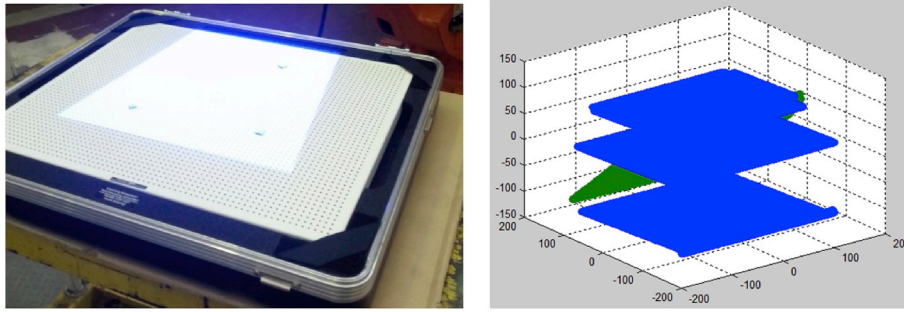


Fig. 6. Experimental calibration of measured planes (mm).



Fig. 7. Experimental calibration of measured spheres.

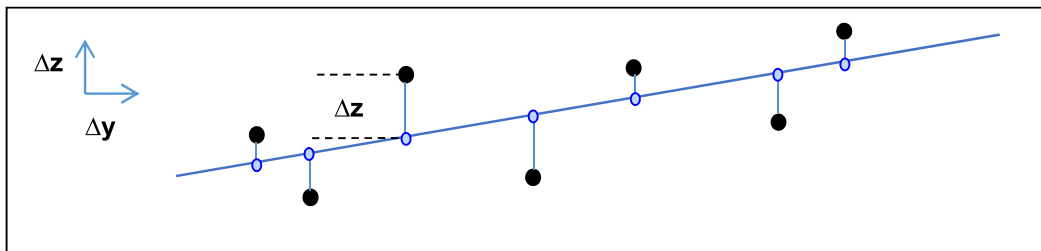
Table 1  
The fitting planes by LS method.

Plane	Number of points	Gauge plane
Lower plane	33678	$z = -122.9953 + 0.00010 * x - 0.0516 * y$
Middle plane	41051	$z = 5.5013 + 0.001953 * x - 0.05085 * y$
Upper plane	31894	$z = 78.7114 + 0.003069 * x - 0.04998 * y$
Diagonal plane	57649	$z = 20.2790 - 0.0125 * x - 0.9290 * y$

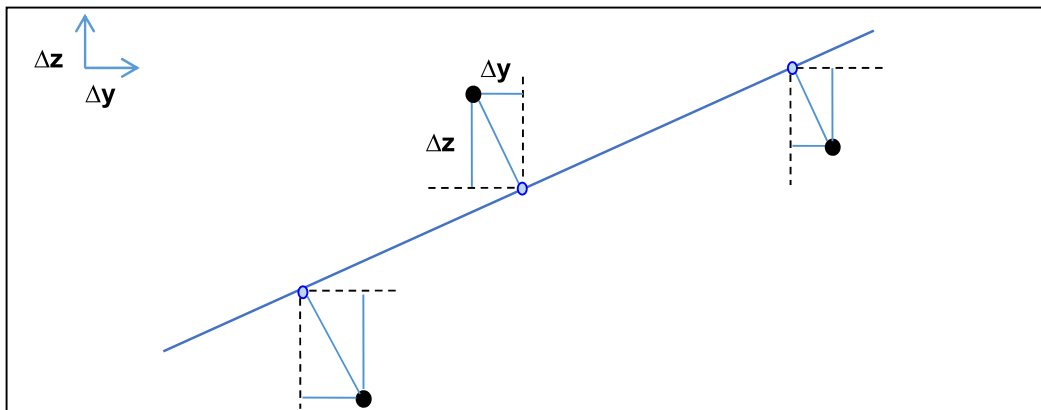
$(\Delta x_i, \Delta y_i, \Delta z_i)$  are calculated by the difference between the measured coordination data and the coordination of the projected points on the gauge plane. For lower, middle and upper planes,  $\Delta z_i$  are calculated, while for diagonal plane,  $\Delta y_i$  and  $\Delta z_i$  are calculated as the measurement errors. The results of measurement errors on different planes are shown in Fig. 9.

3.2.2. Sphere case

The calibrated radius of the gauge sphere is 15.0004 mm, and the coordinate of the sphere center is fitted by LS method using the measured points (see Fig. 10). The theoretical reference sphere (spherical datum surface curve) can be obtained. The measurement errors are the differences between the coordinates of actual measured points and the coordinates of their projection points on the spherical datum surface, expressed by  $(\Delta x_i, \Delta y_i, \Delta z_i)$ . The gauge sphere is shown in Table 2. The



(a) Plane with small angle



(b) Plane with large angle

Fig. 8. Calculation of measurement error on calibration plane.

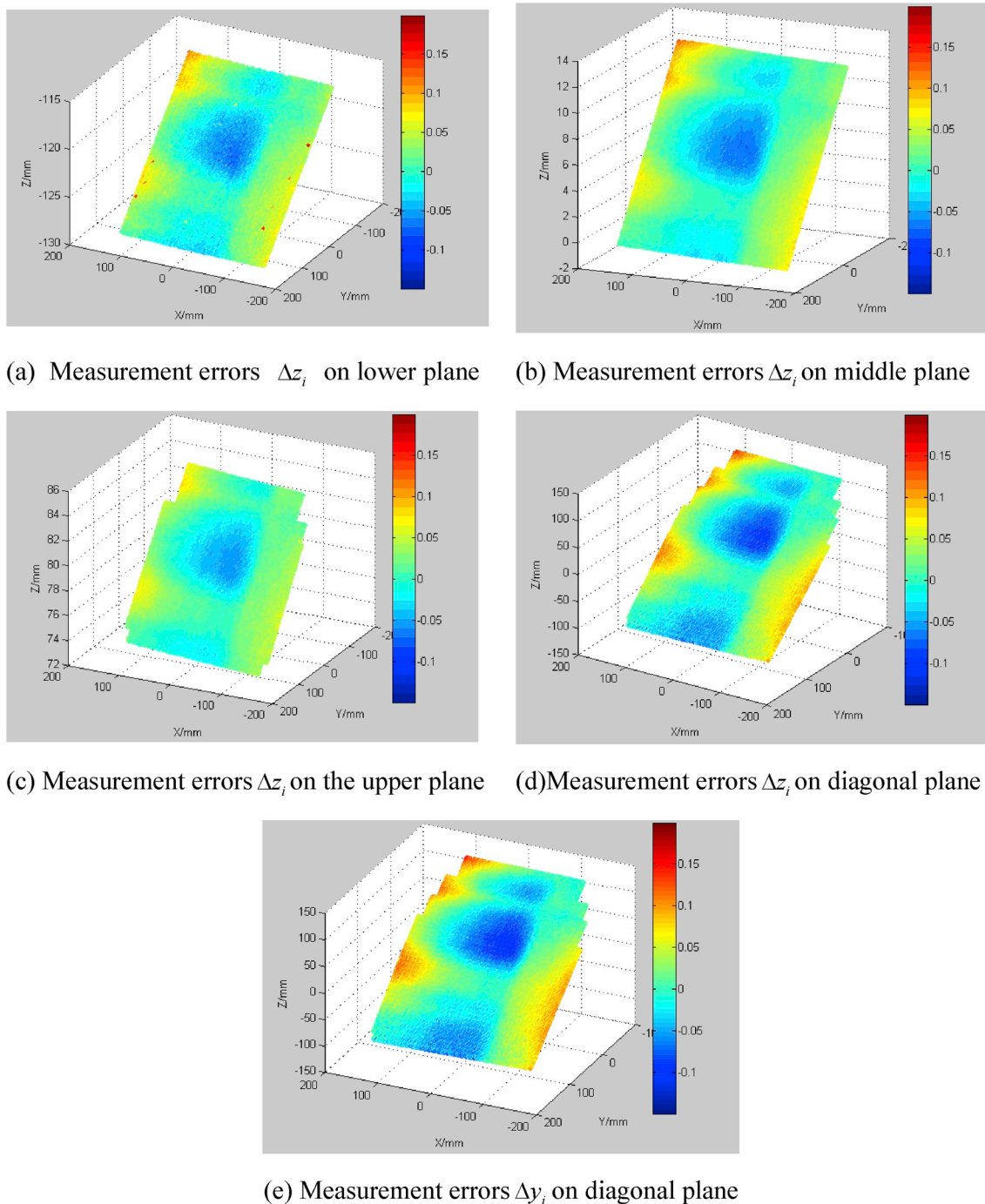


Fig. 9. Measurement errors on different planes (mm).

results of measurement errors on spherical surfaces are shown in Fig. 11. The measurement uncertainty of the calibrated radius of the gauge sphere has an impact on the errors assessment and therefore on the kriging model. GOM gauge was used in this application. The accuracy of the radius form is 0.0012 mm (GOM calibration certificate).

### 3.3. Calibration results and discussion

#### 3.3.1. Plane case

According to the proposed calibration method based on Kriging for GOM sensor, the measurement errors calculated at different sites on the plane are considered as regional variables, and are used to estimate the calibrations in any other sites. For the lower plane, 1000 three

dimensional data and the corresponding measurement errors  $\Delta z_i$  are randomly sampled from 33678 measured points. Two experiments were conducted to provide calibrations in various areas: on the gauge plane and in a larger cubic space around the gauge plane. The measured points are collected and used to estimate the calibrations in Fig. 12.

The process of calibration calculation is explained for the unmeasured points in Fig. 12. For sampling in a larger cubic space, 1,000 points are collected by rectangular grid method in the larger cubic space around the fitting mean plane (Fig. 12 (a)). Then the calibrations of these 1000 points are predicted using previously calculated measurement error data  $\Delta z_i$  selected from 33678 by random sampling method. While sampling on the fitting plane, 2912 (52 \* 56) points are collected by mesh grid method on the fitting mean plane (Fig. 12 (b)).

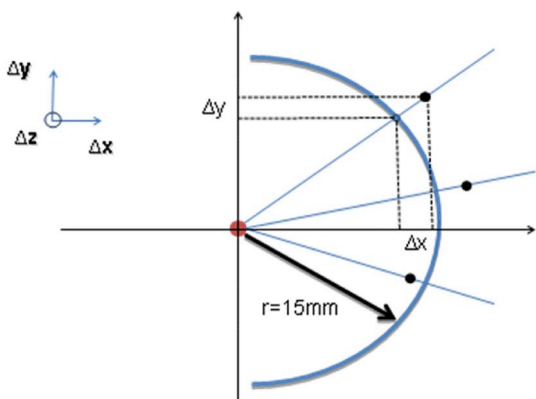


Fig. 10. Calculation of measurement error on calibration sphere.

Table 2  
The fitting sphere by LS method.

	X	Y	Z
Gauge center of sphere	-85.2707	65.6985	-55.4355
Measured radius	15.0088 mm		
Gauge radius	15.0004 mm		

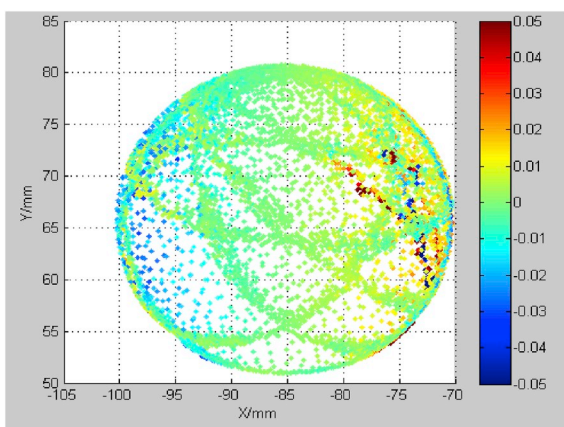
Then the calibrations of these 2912 points are estimated using the same known measurement error data.

To estimate calibrations for sampling on the fitting plane, two methods are defined in the calculation (see Fig. 13). The first one is that the calibration is directly based on the positions of points  $\Delta z_0 = w(x_{i\text{-measured}}, y_{i\text{-measured}}, z_{i\text{-measured}})$  (called direct method). The second one is based on Kriging described as follow. The height value of Z has spatial correlation with the positions X and Y. Thus, the estimation of the value Z is calculated by Kriging Method  $z_0^* = f(x_{i\text{-measured}}, y_{i\text{-measured}})$ . The calibration is obtained by the difference between the estimated value  $z_0$  and the projection point on the fitting plane  $\Delta z_0 = z_0^* (\text{point predicted}) - z$  (point projected on the fitting plane). For the diagonal plane, measurement error along Y axis is calculated in the same way.

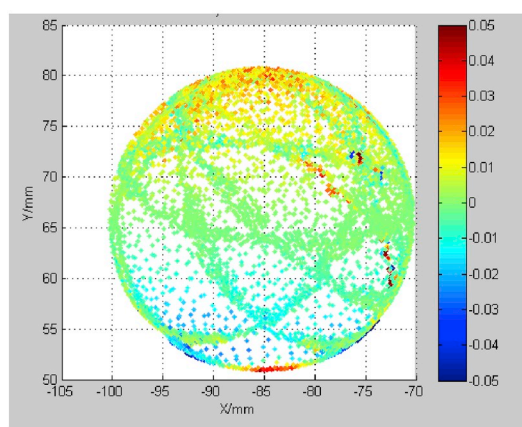
Calibrations in both areas are estimated by the Kriging method, the calibrations  $\Delta z_0$  in the cubic space and on the fitting plane are shown in Fig. 14. The left image shows the estimated calibration, and the right image is the variance of estimation.

The distribution of the estimated calibration depends greatly on the distribution of the measurement error. If the point is closer to the expected measured points, the variance of the estimate is lower. The variance of the estimation in the cubic space is symmetrical along the gauge plane and lower around the gauge plane.

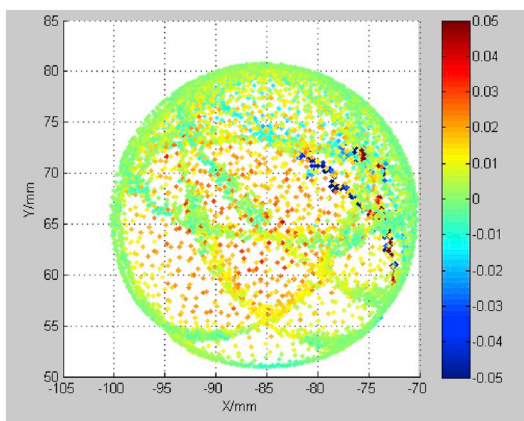
It is important to choose the appropriate Kriging method including correlation model and regression model corresponding to the sampling strategy in order to reduce the estimation variance. Table 3 shows that



(a) The measurement errors of X axis



(b) The measurement errors of Y axis



(c) The measurement errors of Z axis

Fig. 11. Measurement error on the spherical datum surface (mm).

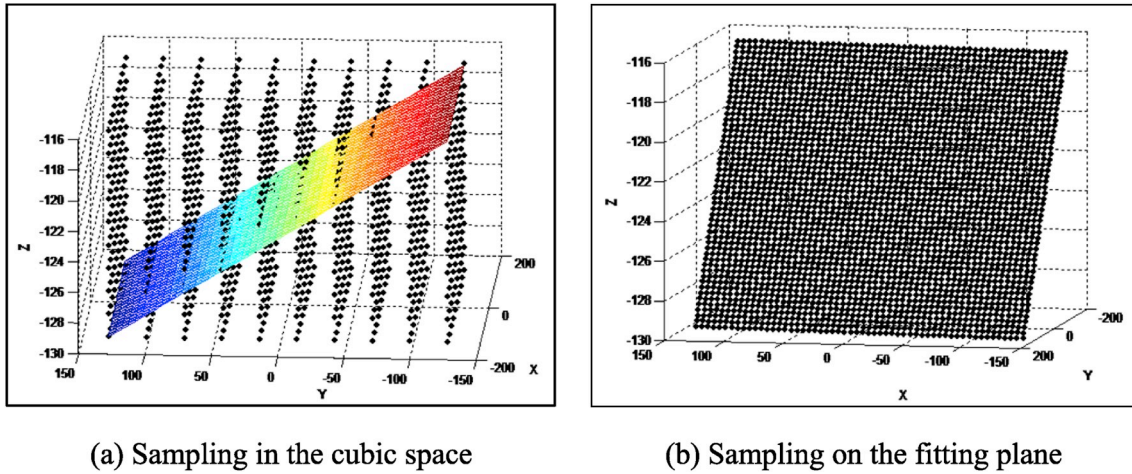


Fig. 12. Spatial sampling for the calibration area.

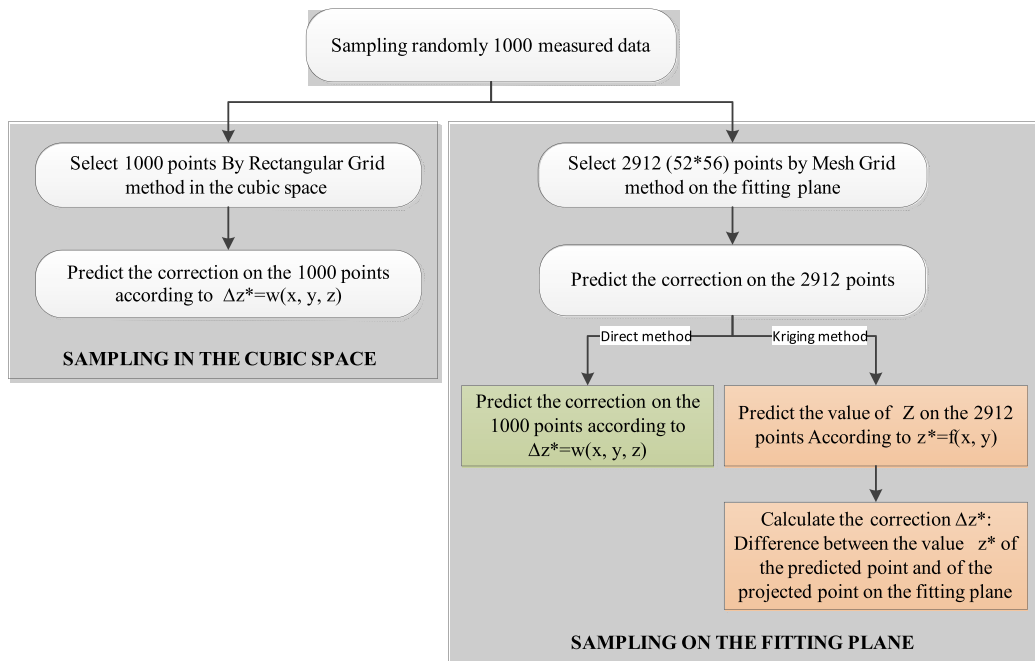


Fig. 13. Flow diagram of the measurement error calibration on datum plane.

the results of estimation and variance in process of calibration. According to Table 3, when the exponential model is chosen as the correlation model and Ordinary Kriging is chosen as the regression model in Fig. 14(a) and (b), and Universal Kriging is chosen in Fig. 14 (c) respectively, the estimation variances  $\sigma_{\frac{z}{2}}^2(s_0)$  are minimized.

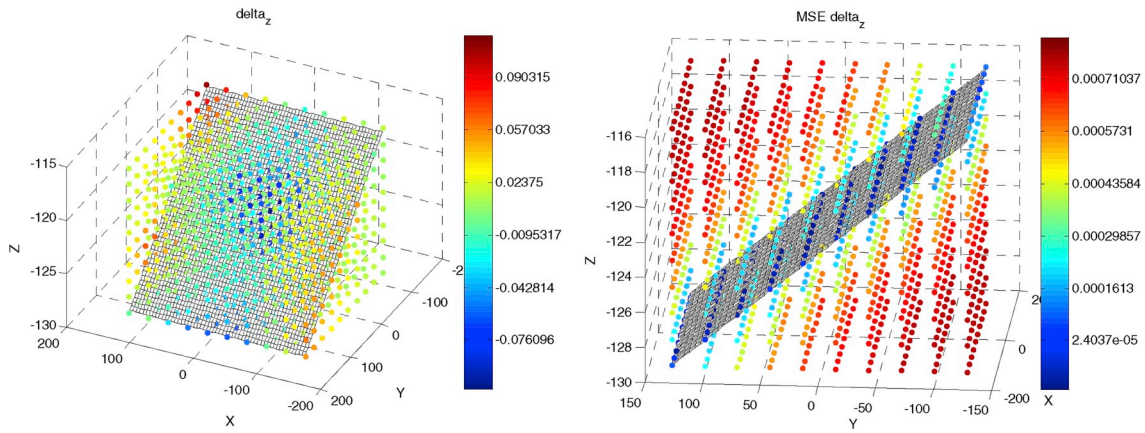
### 3.3.2. Sphere case

Two experiments were conducted to provide calibrations in various areas: in the cubic space and on the gauge sphere shown in Fig. 15. The estimation points on the spherical datum surface are shown in Fig. 16, and results of calibration estimation and estimation error variance on the spherical datum surface are shown in Fig. 17. The calibration of GOM sensor can be achieved at any sites of the full-field area of measurement by the proposed Kriging method. For a new measurement mission, the calibration of the measurement system can be automatically compensated to the results of the measures.

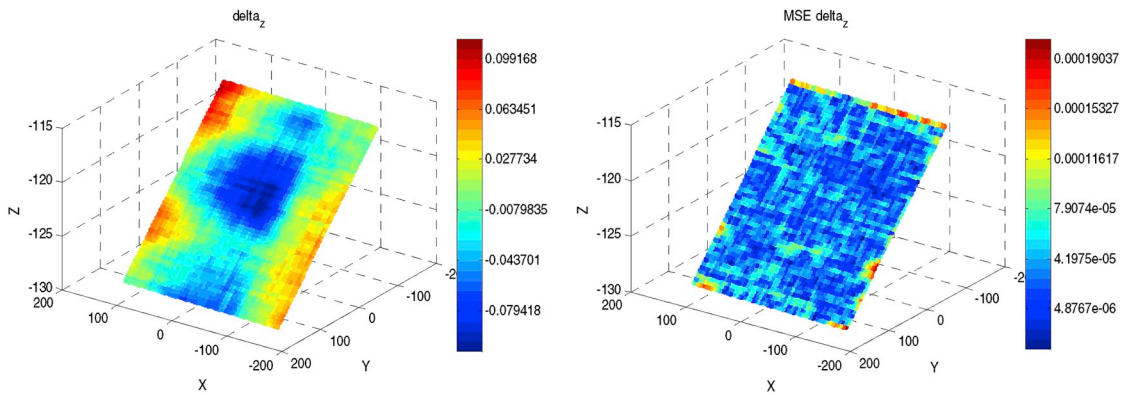
### 3.4. Sensitivity analysis of different numbers of points to construct meta-model

The cross-validation method not only helps to choose the appropriate Kriging method to estimate the calibration of the GOM sensor, but also assists to decide the number of measurement error applied to construct meta-model of calibration. The sensitivity analysis on different initial number of points to construct meta-model is conducted according to the process of cross-validation in Fig. 4, and the main steps are described as follows.

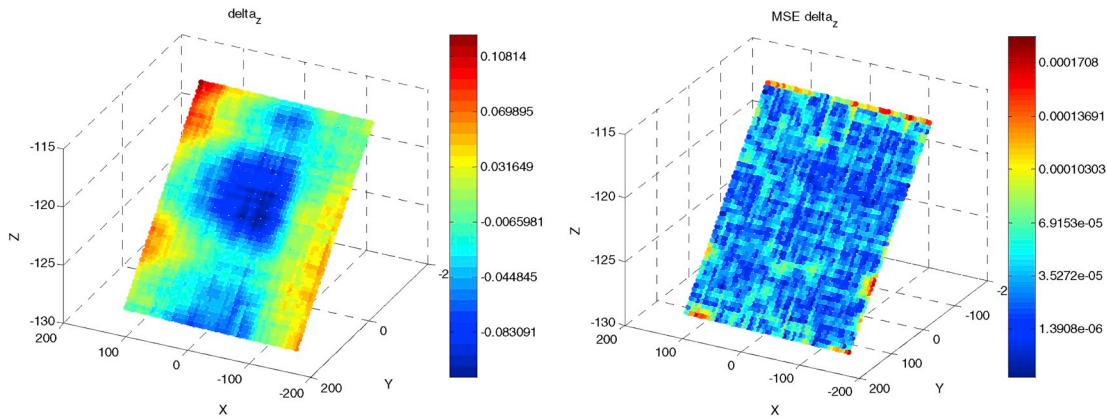
- 1) Generate the measurement error  $\Delta z_i$  by the  $N$  measured points ( $N = 33678$ ).
- 2) Randomly select  $M = 10, 50, 100, 300, 500$  points from the  $N$  measured points for the estimation of calibration and temporarily eliminate the measurement error of the remaining points ( $N-M$ ).
- 3) Calculate the estimation and Kriging variance associated in the



(a) Estimation of the calibration in the cubic space



(b) Estimation of the calibration on the fitting plane by direct method



(c) Estimation of the calibration on the fitting plane by Kriging method

Fig. 14. Result of estimation of the calibration and variance of estimation.

remaining points.

- 4) Repeat 50 times steps (2) to (3) for each M points.
- 5) Calculate the cross-validation criterion
- 6) Build the box plot (box-whisker plot) of cross-validation criterion for evaluation.

Fig. 18 shows the results of different cross-validation criterion ME, MSE, RMSE, AKSE, MSPE and RMSPE with different numbers of measured points for the creation of meta-model Kriging.

According to Fig. 18, some conclusions can be obtained:

- 1) The average estimation errors (ME) and standard errors (MSE) is closer to 0 with the increasing number.
- 2) The variance of estimation errors (MSE, RMSE) is lower with greater number of points. This criterion reflects the robustness of the estimator and information on the accuracy of the estimation.
- 3) The values of MSPE with different numbers of points converge to 0. But RMSPE has a fluctuation with the increasing number of points,

**Table 3**  
Results of estimation and variance in process of calibration.

	In the cubic space		On the fitting plane by Direct method		On the fitting plane by Kriging method	
	Estimation	Variance	Estimation	Variance	Estimation	Variance
Mean			2.08E-04	5.50E-05	2.30E-04	4.99E-05
Min	-7.61E-02	2.40E-05	-7.94E-02	4.88E-06	-8.31E-02	1.39E-06
Max	9.03E-02	7.10E-04	9.92E-02	1.90E-04	1.08E-01	1.71E-04
Regression model	Ordinary Kriging				Universal Kriging	
Correlation model	Exponential model					

and at last converges to the specific value, 1.

Thus, the accuracy of the estimation of calibrations is increased by the number of measured points for the creation of meta-model. But the accuracy is priced by measurement cost and the calculation time. Generally, the more number of points used to estimate the calibration by Kriging method, the higher accuracy of estimation is achieved. So it is important to choose the appropriate number of points for the meta-model creation. The best indication is the variability RMSPE.

- RMSPE = 1 indicates that the prediction of the calibration is correct and effective.
- RMSPE > 1 indicates that the prediction is overestimated, which means to reduce the measurement information.
- RMSPE < 1 indicates that the prediction is underestimated, which means to increase the measurement information.

The variability of RMSPE by Ordinary Kriging and by Universal Kriging are shown in Fig. 19. For Ordinary Kriging, 50 or 100 measured points lead to a less than 1 RMSPE, but for 500 points it is greater than 1. This indicates that 500 measured points are sufficient for the prediction of calibrations. If more points are used for the calculation, the variability of the prediction will be overestimated. For Universal Kriging, 500 measured points are not enough to perform the calibration. For an industrial application, a reference threshold of RMSPE could be defined to optimize the needed number of measured points.

3.5. Spatial correlation analysis for measurement uncertainty

A convenient choice for the correlation function is within the power

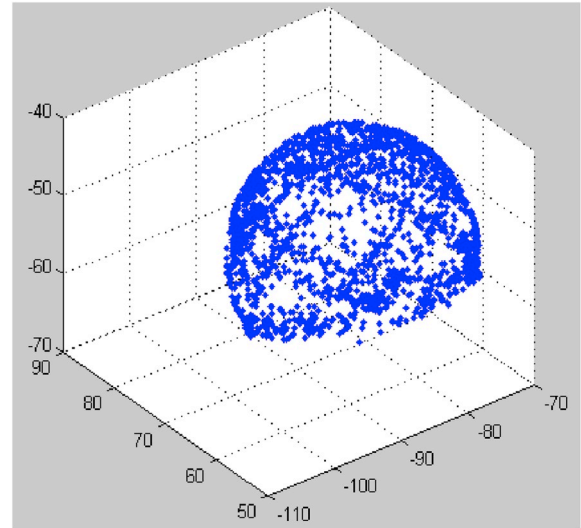
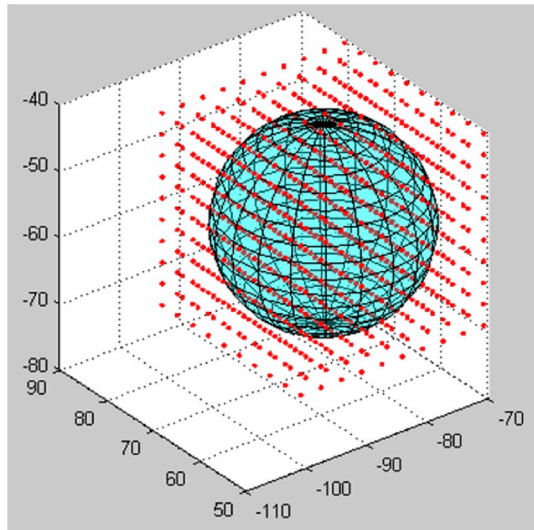


Fig. 16. Estimation points on the spherical datum surface.

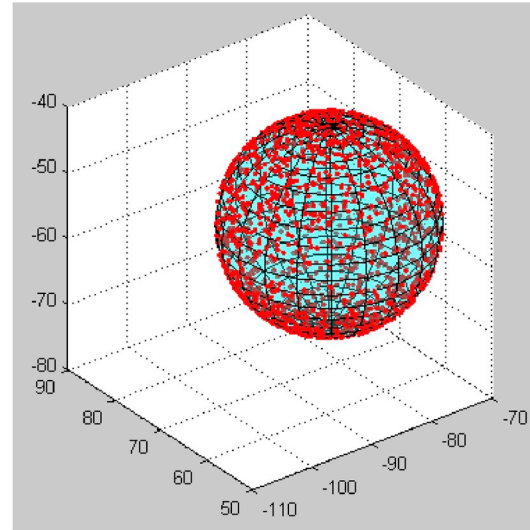
exponential model and spherical model. Spatial correlation functions are  $d = \|s_i - s_j\|$ .

- Exponential model:  $R_j(\theta, d_j) = \exp(-\theta_j |d_j|)$
- Gaussian model:  $R_j(\theta, d_j) = \exp(-\theta_j d_j^2)$
- Spherical model:  $R_j(\theta, d_j) = 1 - 1.5\xi_j + 0.5\xi_j^3, \xi_j = \min\{1, \theta_j |d_j|\}$

Fig. 20 shows the spatial correlation influenced by distance and  $\theta$ .

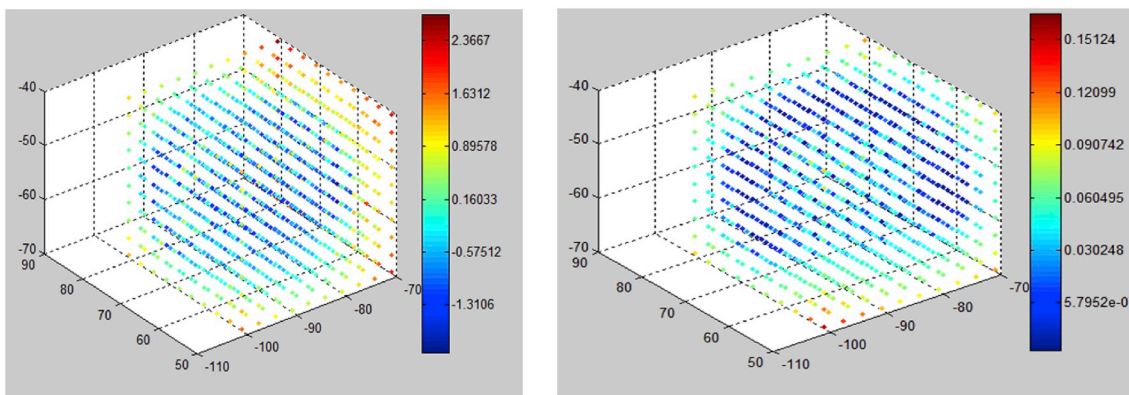


(a) sampling in the cubic space



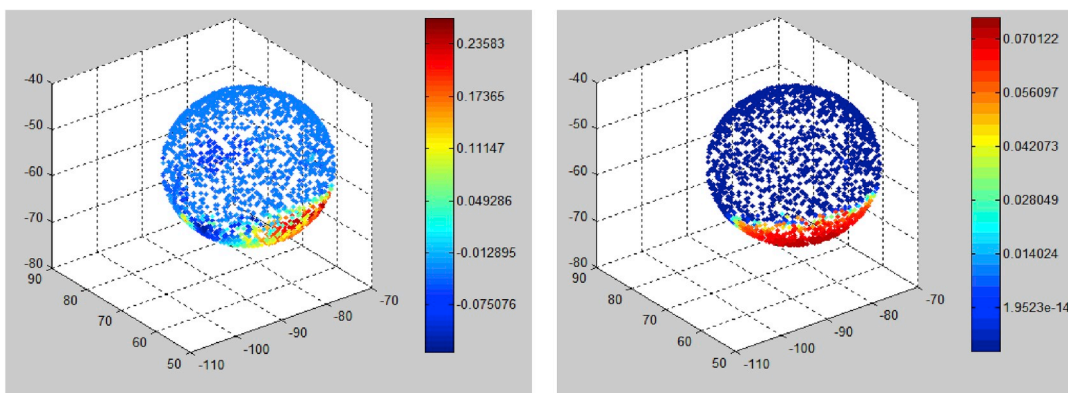
(b) sampling on the fitting sphere

Fig. 15. Spatial sampling for the calibration area.



Calibration at X axis

Prediction variance at X axis



Calibration at Y axis

Prediction variance at Y axis

Fig. 17. Results of calibration estimation and estimation error variance on the spherical datum surface.

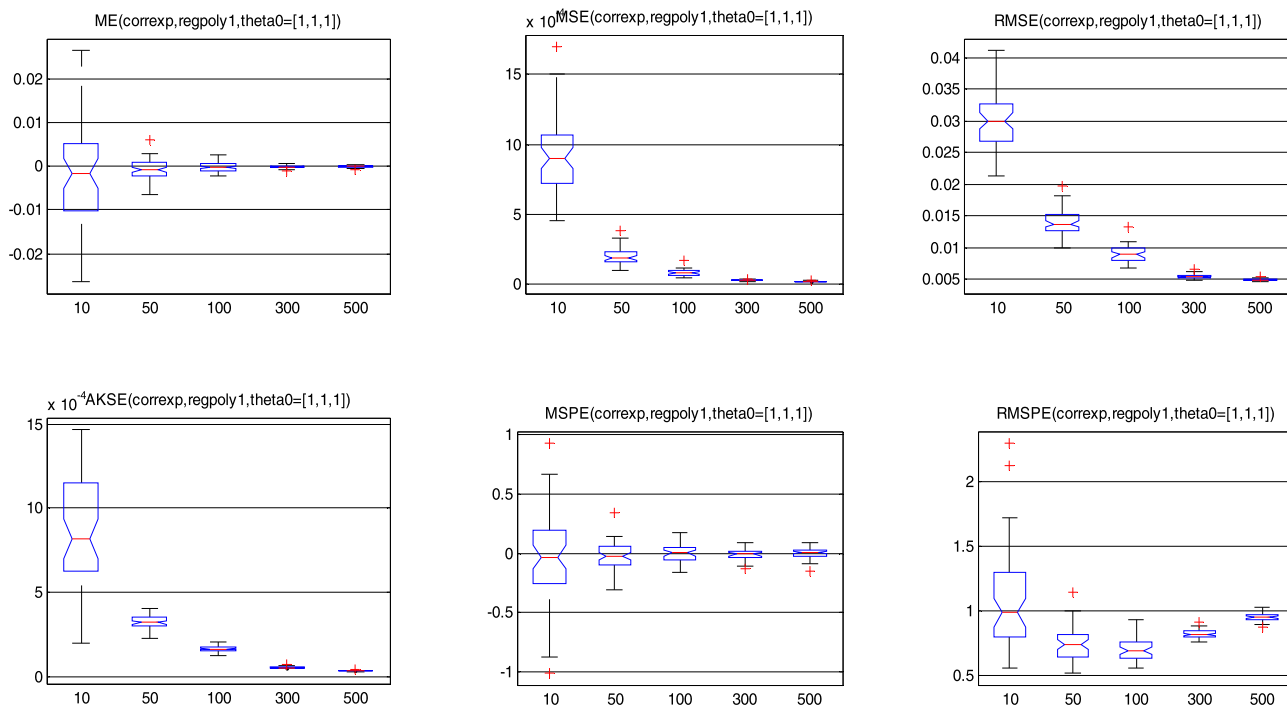


Fig. 18. Box-whisker of cross validation indices.

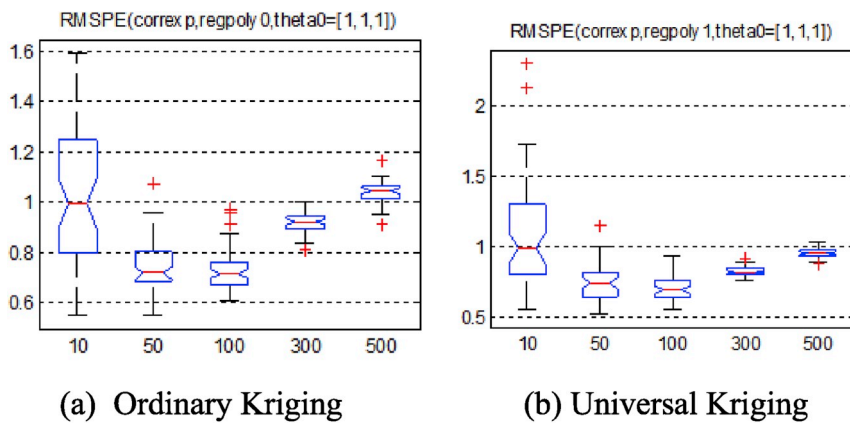


Fig. 19. Results of the comparison of the number of measured points.

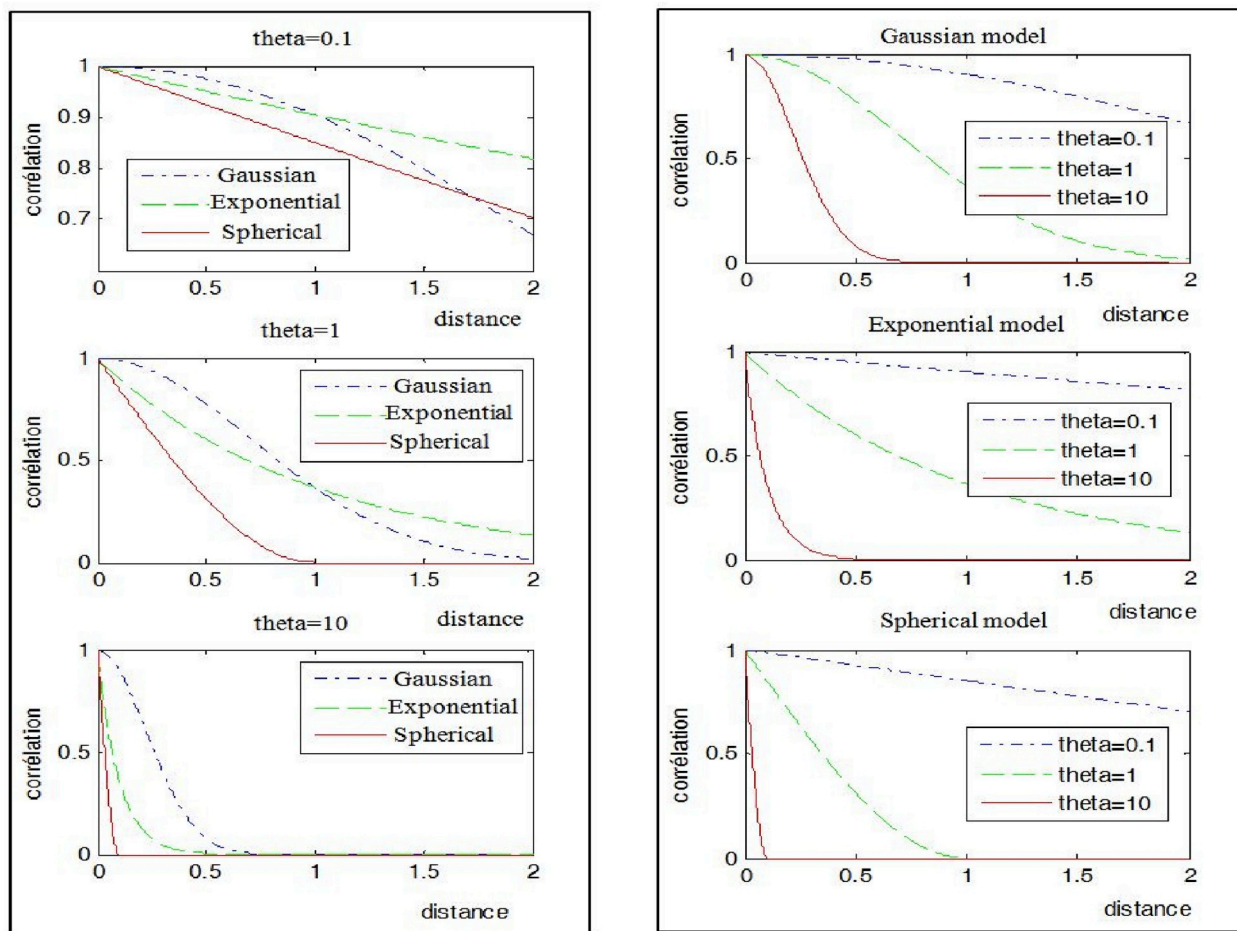


Fig. 20. Spatial correlation influenced by distance and theta.

From Fig. 20, it is observed that the correlation decreases with  $d$  and a larger value for  $\theta$  leads to a faster decrease.

#### 4. Conclusion

In this paper, a novel Kriging models-based calibration and uncertainty estimation method is developed to improve the measurement accuracy of non-contact 3D CMSs. This calibration procedure has been tested on a measurement system with the GOM sensor, which served as a tool of measurement after calibration. The results of calibrations are

used to compensate and correct the measurement system to perform a new measure. The cross-validation technique is applied to select the best Kriging model and decide the initial measured points to create the meta-model. The accuracy of the results and the effective of the calibration estimation impact on the measurement time and on the computation time. The results show that fitted calibration surface obtained through Kriging-based method can provide accurate estimation of the calibration for the new measurement. As shown in Fig. 17, the accuracy of the results with the kriging compensation is 10 times the accuracy of the results without the kriging compensation.

## Appendix A. Supplementary data

Supplementary data to this article can be found online at <https://doi.org/10.1016/j.precisioneng.2019.02.004>.

## References

- [1] Kolen PT. Self-calibration/compensation technique for microcontroller-based sensor arrays. *IEEE Trans Instrum Meas* Aug. 1994;43(9):620–3.
- [2] Bacakoglu H, Kamel MS. A three-step camera calibration method. *IEEE Trans Instrum Meas* Oct. 1997;46(5):1165–72.
- [3] Sansoni G, Carocci M, Rodella R. Calibration and performance evaluation of a 3-D imaging sensor based on the projection of structured light. *IEEE Trans Instrum Meas* Jun. 2000;49(3):628–36.
- [4] Shen TS, Meng CH. Automatic camera calibration for a multiple-sensor integrated coordinate measurement system. *IEEE Trans Robot Autom* Aug. 2001;17(4):502–7.
- [5] Du S, Liu C, Xi L. A selective multiclass support vector machine ensemble classifier for engineering surface classification using high definition metrology. *ASME Trans J Manuf Sci Eng* 2015;137. 011003-1-15.
- [6] Du S-C, Huang D-L, Wang H. An adaptive support vector machine-based workpiece surface classification system using high definition metrology. *IEEE Trans Instrum Meas* 2015;64(10):2590–604.
- [7] Nguyen HT, Wang H, Hu SJ. Characterization of cutting force induced surface shape variation in face milling using high-definition metrology 1. *ASME Trans J Manuf Sci Eng* 2013;135(4):041014–04101412.
- [8] Nguyen H, Wang H, Tai BL, Ren J, Hu SJ, Shih A. High-Definition metrology enabled surface variation control by cutting load balancing. *ASME Trans J Manuf Sci Eng* 2016;138(2). pp. 021010-1-02101011.
- [9] Wang M, Xi L, Du S. 3D surface form error evaluation using high definition metrology. *Precis Eng* 2014;38(1):230–6.
- [10] Du S, Liu C, Huang D. A shearlet-based separation method of 3D engineering surface using high definition metrology. *Precis Eng* 2015;40:55–73.
- [11] Wang M, Shao Y-P, Du S-C, Xi L-f. A diffusion filter for discontinuous surface measured by high definition metrology. *Int J Precis Eng Manuf* 2015;16(10):2057–62.
- [12] Wang M, Ken T, Du S, Xi L. Tool wear monitoring of wiper inserts in multi-insert face milling using three-dimensional surface form indicators. *ASME Trans J Manuf Sci Eng* 2015;137(3):031006–7.
- [13] Pan B, Yu L, Wu D, Tang L. Systematic errors in two-dimensional digital image correlation due to lens distortion. *Optic Laser Eng* 2013;51(2):140–7.
- [14] Cui S, Zhu X. A generalized reference-plane-based calibration method in optical triangular profilometry. *Optic Express* 2009;17(23):20735–46.
- [15] Pan B, Yu L, Wu D, Tang L. Systematic errors in two-dimensional digital image correlation due to lens distortion. *Optic Laser Eng* 2013;51(2):140–7.
- [16] Huang PS, Ni J. On-line error compensation of coordinate measuring machines. *Int J Mach Tool Manuf* 1995;35(5):725–38.
- [17] Sato O, Osawa S, Kondo Y, Komori M, Takatsuji T. Calibration and uncertainty evaluation of single pitch deviation by multiple-measurement technique. *Precis Eng* 2010;34(1):156–63.
- [18] Barini EM, Tosello G, De Chiffre L. Uncertainty analysis of point-by-point sampling complex surfaces using touch probe CMMs. *Precis Eng* 2010;34(1):16–21.
- [19] Hong C, Ibaraki S. Non-contact R-test with laser displacement sensors for error calibration of five-axis machine tools. *Precis Eng* 2013;37(1):159–71.
- [20] Kajima M, Minoshima K. Calibration of linear encoders with sub-nanometer uncertainty using an optical-zooming laser interferometer. *Precis Eng* 2014;38(4):769–74.
- [21] Evans CJ. Precision engineering: an evolutionary view. Cranfield, U. K.: Cranfield University Press; 1989.
- [22] Chen YD, Ni J. Dynamic calibration and compensation of a 3D laser radar scanning system. *IEEE Trans Robot Autom* Jun. 1993;9(3):318–23.
- [23] Caja J, Gómez E, Maresca P. Optical measuring equipments. Part I: calibration model and uncertainty estimation. *Precis Eng* 2015;40:298–304.
- [24] Shen Y, Moon S. Error compensation of coordinate measurements in computer-Integrated manufacturing using neural networks. *J Mater Process Technol* 1996;61(1–2):12–7.
- [25] Yang Q, Butler C, Baird P. Error compensation of touch trigger probes. *Measurement* 1996;18(1):47–57.
- [26] Dong C, Zhang C, Wang B, Zhang G. Prediction and compensation of dynamic errors for coordinate measuring machines. *ASME Trans J Manuf Sci Eng* 2002;124(3):509–14.
- [27] Tan KK, Huang SN, Seet HL. Geometrical error compensation of precision motion systems using radial basis function. *IEEE Trans Instrum Meas* Oct. 2000;49(5):984–91.
- [28] Tan KK, Huang SN, Lee TH. Dynamic S-function for geometrical error compensation based on neural network approximations. *Measurement* Sep. 2003;34(2):143–56.
- [29] Barakat NA, Elbestawi MA, Spence AD. Kinematic and geometric error compensation of a coordinate measuring machine. *Int J Mach Tool Manuf* 2000;40(6):833–50.
- [30] Li XH, Chen B, Qiu ZR. The calibration and error compensation techniques for an articulated arm CMM with two parallel rotational axes. *Measurement* 2013;46(1):603–9.
- [31] Bai Y, Zhuang H. On the comparison of bilinear, cubic spline, and fuzzy interpolation techniques for robotic position measurements. *IEEE Trans Instrum Meas* Dec. 2005;54(6):2281–8.
- [32] Teo C-S, Tan K-K, Lim S-Y. Dynamic geometric compensation for gantry stage using iterative learning control. *Int J Mach Tool Manuf* 2008;57(2):413–9.
- [33] Yang SL, Xu KJ. Numerical Derivation-based serial iterative dynamic decoupling-compensation method for multi-axis force sensors. *IEEE Trans Instrum Meas* Dec. 2014;63(12):2950–62.
- [34] Wei J, Chen Y. The geometric dynamic errors of CMMs in fast scanning-probing. *Measurement* 2011;44(3):511–7.
- [35] Wen X-l, Zhao Y-b, Wang D-x, Pan J. Adaptive Monte Carlo and GUM methods for the evaluation of measurement uncertainty of cylindricity error. *Precis Eng* 2013;37(4):856–64.
- [36] Feng H-Y, Liu Y, Xi F. Analysis of digitizing errors of a laser scanning system. *Precis Eng* 2001;25(3):185–91.
- [37] Isheil A, Gonnet JP, Joannic D, Fontaine JF. Systematic error correction of a 3D laser scanning measurement device. *Optic Laser Eng* 2011;49(1):16–24.
- [38] Johnson RP, Qingping Yang Q, Butler C. Dynamic error characteristics of touch trigger probes fitted to coordinate measuring machines. *IEEE Trans Instrum Meas* Oct. 1998;47(5):1168–72.
- [39] Pereira PH, Hocken RJ. Characterization and compensation of dynamic errors of a scanning coordinate measuring machine. *Precis Eng* 2007;31(1):22–32.
- [40] Schwenke H, Knapp W, Haitjema H, Weckenmann A, Schmitt R, Delbressine F. Geometric error measurement and compensation of machines—an update. *CIRP Ann - Manuf Technol* 2008;57(2):660–75.
- [41] Zhang GX, Zhang HY, Guo JB, Li XH, Qiu ZR, Liu SG. Error compensation of cylindrical coordinate measuring machines. *CIRP Ann - Manuf Technol* 2010;59(1):501–4.
- [42] Suriano S, Wang H, Shao C, Hu SJ, Sekhar P. Progressive measurement and monitoring for multi-resolution data in surface manufacturing considering spatial and cross correlations. *IIE Trans* 2015;47(10):1033–52.
- [43] Poniatowska M. Research on spatial interrelations of geometric deviations determined coordinate measurements of free-form surfaces. *Metrol Meas Syst* 2009;16(3):501–10.
- [44] Chen X, Ankenman BE, Nelson BL. Enhancing stochastic Kriging metamodelling with gradient estimators. *Oper Res* 2013;61(2):512–28.
- [45] Kleijnen JPC. Kriging metamodelling in simulation: a review. *Eur J Oper Res* 2009;192(3):707–16.
- [46] Du S, Fei L. Co-Kriging method for form error estimation incorporating condition variable measurements. *ASME Trans J Manuf Sci Eng* 2016;138. 041003-1-16.
- [47] Ascione R, Moroni G, Petro S, Romano D. Adaptive inspection in coordinate metrology based on kriging models. *Precis Eng* 2013;37(1):44–60.
- [48] Dumas A, Echard B, Gayton N, Rochat O, Dantan JY, Van Der Veen S. AK-ILS: an active learning method based on Kriging for the inspection of large surfaces. *Precis Eng* 2013;37(1):1–9.
- [49] Chen Y, Gao J, Deng H, Zheng D, Chen X, Kelly R. Spatial statistical analysis and compensation of machining errors for complex surfaces. *Precis Eng* 2013;37(1):203–12.
- [50] Fan K, Yang J, Yang L. Unified error model based spatial error compensation for four types of CNC machining center: Part II—unified model based spatial error compensation. *Mech Syst Signal Process* 2014;49(1–2):63–76.
- [51] Fan K, Yang J, Yang L. Unified error model based spatial error compensation for four types of CNC machining center: Part I—singular function based unified error model. *Mech Syst Signal Process* 2015;60–61(1–2):656–67.